Structural, Morphological and Optical Study of Manganese Doped FeS (Mackinawite) Nanostructures by Chemical Bath Deposition (CBD) Technique

Sufian Yaqoob[1], Noor ul Hasan[1], Sadia Khalid[2] and Muhammad Saeed Akhtar[1,*]

[1]*Department of Physics, University of Education, 54770, Lahore*

[2]*Nanosciences & Technology Department, National Centre for Physics, Islamabad, Pakistan*

Abstract: $Fe_{1-x}Mn_xS$ thin films with concentration $x=0.02, 0.04, 0.06, 0.08, 0.1$ have been deposited on glass substrates by a simple Chemical Bath Deposition (CBD) method at 90 ^{o}C. The X-ray Diffraction analysis of deposited thin films revealed the growth of mono-phasic mackinawite (FeS) structure with crystallite size in the range from 4.06 to 5.95 nm as a function of manganese concentrations. The other structural parameters like stacking faults, dislocation density and lattice strain affirmed the improvement in crystal structure and phase stability in manganese doped FeS thin films. Scanning Electron Micrographs depicted the growth of nano-flakes and nano-flowers in case of pure FeS thin films while for manganese doped iron sulfide thin films, homogeneity of the deposited material was observed to improve with distinct boundaries of almost spherical nanostructures. The direct energy band gap of FeS mono-phasic thin films was observed to decrease from 2.23 to 1.89 eV as the concentration of manganese increases in host lattice. The prepared thin films with tunable optical properties would have potential applications in energy conversion and optoelectronic devices.

Keywords: Thin films, Mackinawite FeS, Nano-flakes, Optoelectronics.

1. INTRODUCTION

In recent years, thin films of doped semiconductors have been arising revolution in optoelectronics and energy applications because of thickness from nanometer to few micrometer range when deposited on variety of substrate [1]. The characteristics of thin films depend upon the growth techniques where the properties of thin films are tuned. Thin films of metal chalcogenides family especially iron sulfide have potential attraction due to their viability in energy storage and energy conversion applications [2-4]. There are several theoretical investigations on optical and structural properties of chalcogenide materials emphasized the importance of these materials for optical and optoelectronic devices [5-8]. Iron sulfide is an important semiconductor material due to its natural abundance, low-cost synthesis and existence in different phases like mackinawite, greigite, pyrhotite, troilite, marcasite and pyrite [9-13]. These phases of iron sulfide are switched attractively from one phase to another under different considerations *e.g.* temperature, pH value, precursors, synthesis routes and environmental interaction [14-16]. The mackinawite ($Fe_{1+x}S$) with excess of iron is an important phase of FeS system due to its mono-phasic nature [17]. It belongs to space group P4/nmm [18], with lattice constants $a=b=3.65$ Å & $c=5.03$ Å [19] and can exhibit interesting optical properties compared to other phases of iron sulfide [20]. Mackinawite FeS occupies anti-PbO like structure [21] in which iron and sulphur are bonded through van-der Waal forces and form tetrahedral edge sharing layers [15]. Mackinawite FeS found naturally in anoxic environment and can be synthesized intentionally using different methods. There are numerous approaches reported for the synthesis of nanocrystalline mackinawite FeS like reacting the iron wire and different ferrous solutions with sulfide solutions [14, 19, 22-26], solvothermal treatment [27], wet chemical reduction technique [28] and techniques used for deposition of thin films of mackinawite FeS *e.g.* vacuum deposition technique [29], electro-deposition [30], spray pyrolysis [31] and chemical bath deposition [32]. Control over the phase of mackinawite FeS thin films during synthesis is a big challenge in present days due to its thermal instability and highly reactive nature towards environment [33]. Many researchers have reported synthesis of nanocrystalline mackinawite at low temperature and standard pressure by the reaction of iron wire with various sulfide solutions and observed the formation of different phases depending on the effect of precursors, temperature, aging time and reducing environment [14, 15]. Sines *et al.* synthesized mackinawite FeS using solvothermal treatment and observed that its crystallinity increased when thermal treatment applied on amorphous mackinawite but other phases were also dominated. It was also observed that material with high purity and stability in phase showed dominant

*Address correspondence to this author at the Department of Physics, University of Education, 54770, Lahore;
E-mail: saeed.akhtar@ue.edu.pk

E-ISSN: 2410-4701/22 © 2022 Zeal Press

properties [27]. Akhtar *et al.* synthesized mono-phasic iron sulfide (mackinawite) thin films using chemical bath deposition process with large optical direct band gap [32]. Malek *et al.* synthesized mackinawite nanoparticles using wet chemical reduction method and investigated the change in optical properties as a function of crystallite size [28]. Kwon *et al.* reported theoretically via Density Functional Theory (DFT) that crystallinity, crystal structure stability and phase of FeS can be controlled by doping suitable transition metals in the crystal structure of mackinawite [33]. Arakaki and Morse also proposed that manganese doped mackinawite provide suitable change in the outcome of structure and chemical properties of mackinawite [34]. In this work, deposition of transition metal doped mackinawite FeS thin films was the matter of interest owing to their applications in solar cells and photovoltaic devices. There are few reports published to date, on transition metal doped mackinawite, and most of them studied the samples in bulk form. Zavasnik *et al.* prepared copper (Cu) doped mackinawite by solvothermal method and reported that Cu doped mackinawite exhibited structural stability with low contents of Cu-ions [35]. Wilkin and Beak (2017) have synthesized Ni doped mackinawite (FeS) in batch experiments under anoxic conditions and reported that phase transformation can occur in samples when interacted with environment and aged with poly-sulfide solutions [36].

In present work, pure and manganese doped FeS (mackinawite) thin films were deposited on glass substrates by chemical bath deposition process for the first time as per our knowledge. The focus of the study is to investigate structural, morphological and optical characteristics of manganese doped mackinawite FeS thin films that can be tuned with different doping concentrations of manganese. In this context, the structural and phase control analysis of mackinawite FeS thin films due to doping of manganese and to utilize it in energy conversion devices such as solar cell is the core theme of this paper. Even though many researchers worked on the mackinawite FeS nanocrystalline and few on mackinawite FeS thin films, yet these manganese doped mackinawite FeS thin films are never studied under current parameters.

2. EXPERIMENTAL METHODOLOGY

2.1. Chemicals

All reagents of Sigma-Aldrich, anhydrous manganese dichloride ($MnCl_2$), iron chloride tetrahydrate ($FeCl_2.4H_2O$), thioacetamide (CH_3NH_2S) and urea (N_2H_4CO) were used without any additional purification in all experiments. The glass substrates of size 1.5 × 2.5 cm^2 were used for the deposition of thin films. The surface of glass substrates was cleaned in ultra-sonic bath with acetone and iso-propyl alcohol for 10 minutes each and dried at room temperature.

2.2. Deposition of Thin Films

Thin films of $Fe_{1-x}Mn_xS$ with $x=0.02, 0.04, 0.06, 0.08$ and 0.1 were deposited on glass substrates by chemical bath deposition method. The chemicals such as $FeCl_2.4H_2O$ (0.15M) for Iron contents, CH_3NH_2S (2M) for Sulphur contents and $(NH_2)_2CO$ (1M) as a complexing agent were dissolved separately in deionized water to prepare 20 mL solution of each precursor. The solution (10 mL) of $MnCl_2$ (0.15 M) was prepared in deionized water to be used as dopant in the experiment. The solutions of iron, thioacetamide and urea were mixed under vigorous stirring to obtain homogeneous reaction mixture of 60 mL followed by the addition of manganese with 0.02, 0.04, 0.06, 0.08 and 0.1 concentrations to perform five different experiments. The final solution mixture was then poured into the jacketed beaker. The temperature of thermostat water bath was fixed digitally at 90^{o}C. Initially the color of reaction mixture was light orange as shown in Figure **1**(**a**) that turned into light black color after 20 minutes of reaction at 90^{o}C as shown in Figure **1**(**b**) indicated the start of nucleation. The color of solution turned entirely black (Figure **1**(**c**)) after 30 minutes of reaction at 90^{o}C. The pre-cleaned glass substrates were dipped vertically with the help of Teflon substrate holder into the jacketed beaker containing reaction mixture as the nucleation started. The substrates were removed from the reaction bath after three hours, washed with deionized water to detach the weakly adhered particles and dried in ambient conditions before further characterizations [32].

Bruker-D8 Advance Diffractometer with Cu-Kα radiations was used for diffraction measurements for 2θ values from 20-80 degrees. The micrographs were obtained by Philips-XL30 scanning electron microscope to analyze the microstructure and surface morphology of thin films. The reflectance spectra were taken by DRA-2 UV-Vis integrating sphere Diffuse Reflectance spectroscopy. The flow chart for the synthesis procedure is given to understand the overall research methodology.

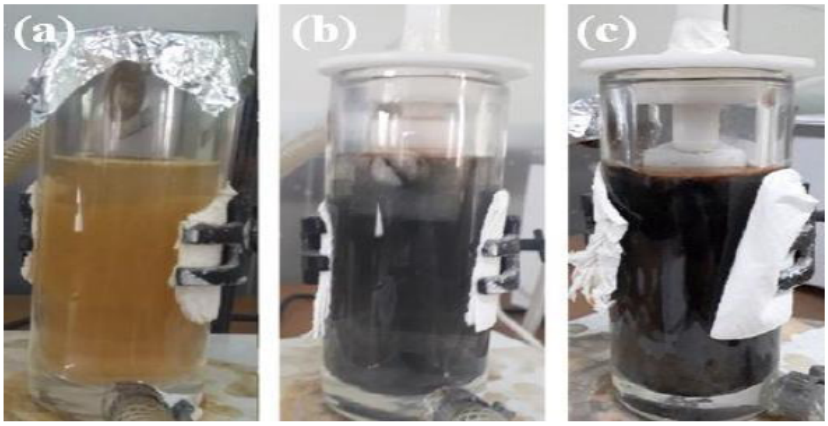

Figure 1: Color of solution (**a**) initially (**b**) after 20 minutes (**c**) after 3 hours.

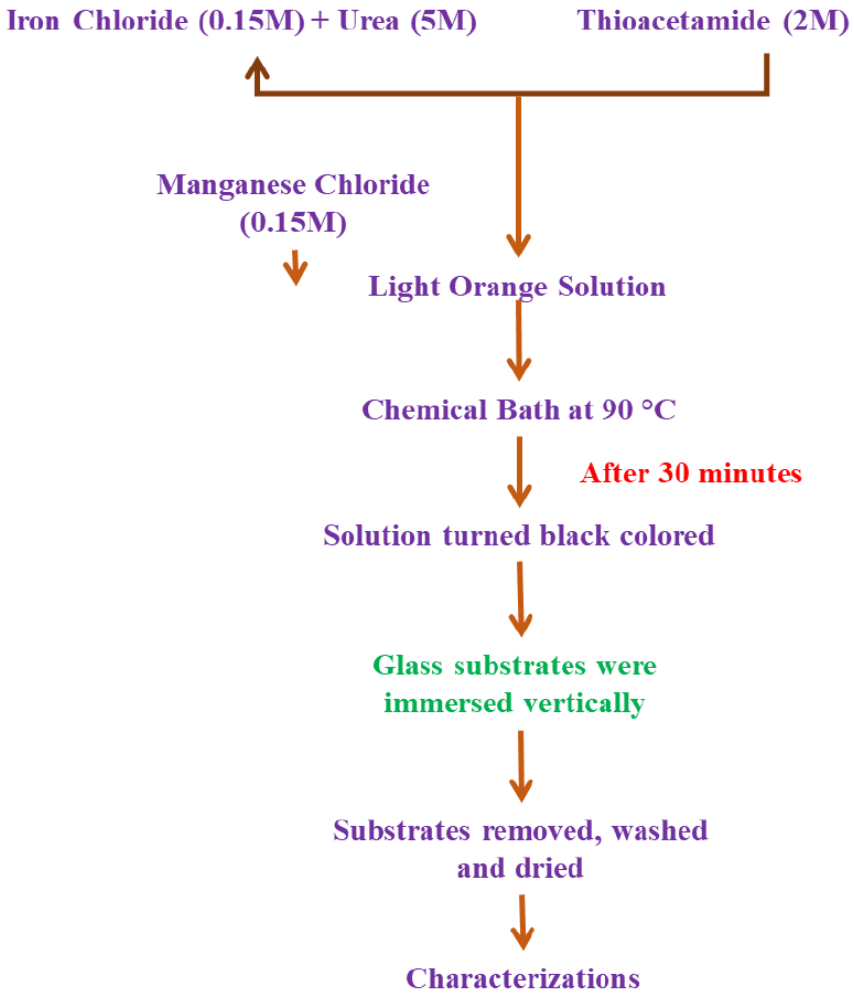

3. RESULTS AND DISCUSSION

3.1. Structural Analysis

X-rays diffraction pattern of pure and manganese doped FeS (mackinawite) thin films are obtained at room temperature and given in Figure **2**. It can be seen that diffraction peak at 2θ value of 17.5 degree correspond to (001) plane and the pattern is consistent with ICDD # 01-086-0389, exhibiting tetragonal crystal structure of mackinawite FeS. The diffraction pattern shows single and broad peak for each sample with different concentration of manganese revealing that there is no presence of any other phase of FeS and

impurities. A slight suppression in intensity of diffraction peak with increasing concentration of manganese would result from inclusion of stacking faults and uneven deposition of thin films as a function of manganese concentration [37]. As the doping concentration increases, a minor shift in diffraction peak towards smaller 2θ values is evident since manganese Mn-ions have large atomic radii (0.08 nm) as compared to Fe-ions (0.074 nm) [37]. The crystalline size of FeS (mackinawite) thin films observed to improve as a function of increasing Mn-contents. Different structural parameters were calculated and listed in Table **1** as literature suggested that manganese doping may provide suitable improvement in chemical and structural properties of mackinawite [34]. The Scherrer's equation was used to estimate the crystallite size as given below:

$$D = \frac{k\lambda}{\beta \cos\theta} \tag{1}$$

Crystallite size (D), shape factor (k=0.98), X-rays wavelength (λ=1.5405Å), β as Full width at half maximum (FWHM) and Bragg Diffraction angle (θ) are illustrated in equation 1 [38]. The average crystallite size was observed in the range from 4.06 to 5.95 nm. The observed change in other structural parameters of mackinawite FeS thin films in lieu of Mn-ions concentration *i.e.* dislocation density, stacking fault, lattice constant, micro and lattice strain are given in Table **1**.

The structural parameters *i.e.* lattice constant 'c' was calculated using relation and represented in Table **1**.

$$\frac{1}{d^2} = \frac{h^2 + k^2}{a^2} + \frac{l^2}{c^2} \tag{2}$$

Here, miller indices are represented by h, k and l for (001) plane similar to those reported in standard data, lattice constants are represented by 'a' and 'c' and d is inter-planer distance. Figure **3** shows a linear relation of lattice constant and crystallite size with manganese concentration.

The variation in dislocation density and lattice strain (ε) is depicted in Figure **4**. It has been observed that crystalline defects were reduced due to well substitution of manganese atoms in place of Fe in the FeS lattice. The dislocation density was calculated using formula:

$$\textbf{\textit{Dislocation Density}} = \frac{1}{D^2} \tag{3}$$

Here, crystallite size is denoted by D. The lattice strain was measured using relation as given below:

$$\varepsilon = \frac{\beta}{4\tan\theta} \tag{4}$$

Here, lattice strain is represented by ε, FWHM is represented by β and θ denote the diffraction angle.

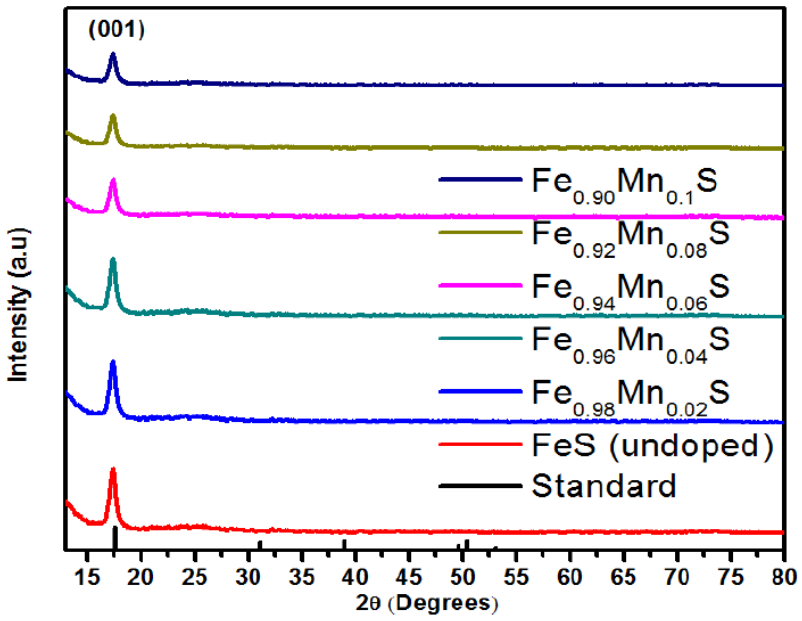

Figure 2: XRD spectra of $Fe_{1-x}Mn_xS$ thin films.

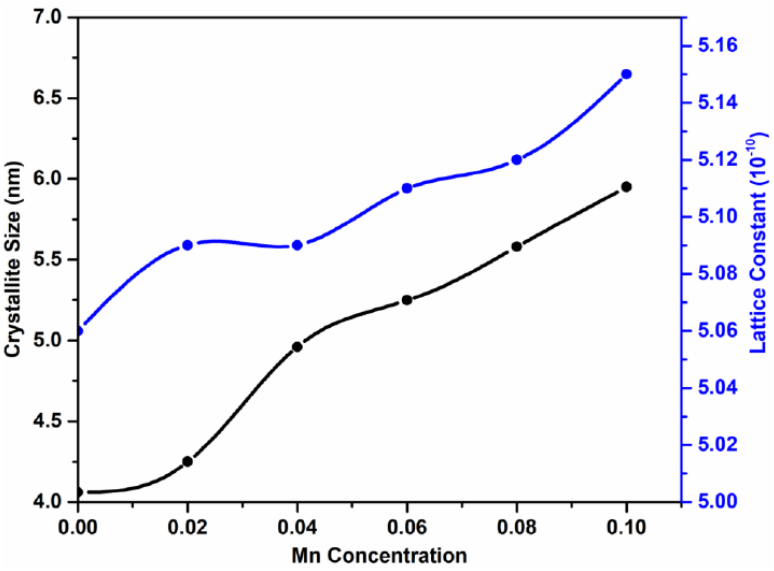

Figure 3: Variation in Crystallite size and Lattice constant as function of Mn-Concentration.

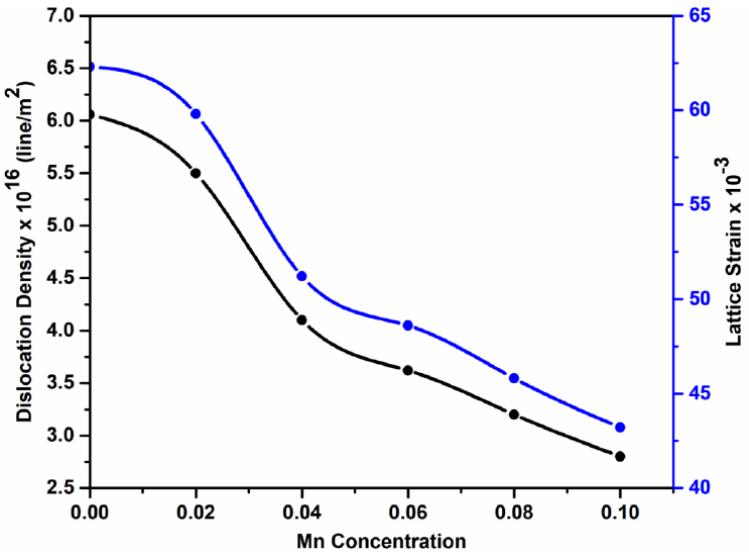

Figure 4: Variation in Dislocation Density and Lattice Strain with Mn-Concentration.

The micro strain (ε_0) was calculated by given relation:

$$\varepsilon_0 = \frac{\beta cos\theta}{4} \quad (5)$$

Here, β is FWHM and diffraction angle is denoted by θ.

Stacking faults were estimated by using formula as mention below:

$$\textbf{Stacking fault} = \frac{2\pi^2}{45\sqrt{3\tan\theta}} \quad (6)$$

Here, θ is diffraction angle. Figure **5** shows the reciprocal trend of micro strains and stacking faults as function of Mn-concentrations. It has been observed that a slight increase in stacking faults would result from fewer plane defects originated in mackinawite FeS crystal structure after doping with manganese.

3.2. Surface Morphology

Thin films were characterized using Scanning Electron Microscope (SEM) to investigate the surface morphology and microstructure. Figure **6** (**a**-**f**) shows SEM micrographs of pure and Mn doped FeS thin films

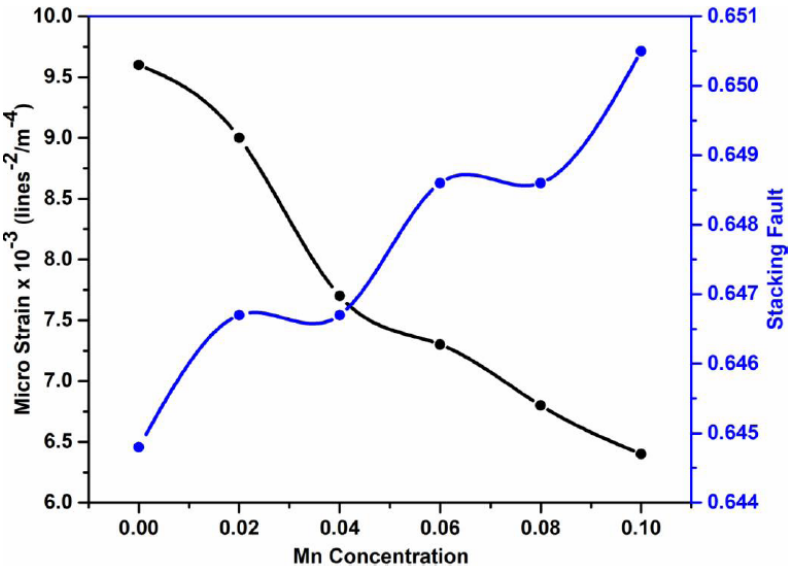

Figure 5: Variation in Micro Strain and Stacking Fault as function of Mn-Concentration.

Table 1: Structural Properties *e.g.* Crystallite Size, Dislocation Density, Lattice Constant, Stacking Fault, Lattice Strain, Micro Strain and Optical Band Gap Values

Mn-Contents	Crystallite Size (nm)	Lattice Constant (Å)	Dislocation Density x 10^{16} (lines/m^2)	Lattice Strain x 10^{-3}	Stacking Fault	Micro Strain x 10^{-3} (lines^{-2}/m^{-4})	Energy Band Gap (eV)
0	4.06	5.06	6.06	62.3	0.6448	9.6	2.23
0.02	4.25	5.09	5.5	59.8	0.6467	9.0	2.21
0.04	4.96	5.09	4.1	51.2	0.6467	7.7	2.13
0.06	5.25	5.11	3.62	48.6	0.6486	7.3	2.09
0.08	5.58	5.12	3.20	45.8	0.6486	6.8	1.98
0.1	5.95	5.15	2.8	43.2	0.6505	6.4	1.89

composed of nano-flakes, nano-flowers and nanoparticles with the dimension in the range from 83 to ≥ 500 nm. The nano flakes and nanoflowers like structures for pure FeS with average length of 132 nm can been seen in Figure **6**(**a**) that reduced after small addition of manganese content *i.e.* x=0.02 [32]. The dimensions of all of nano-flakes were observed to reduce from 132 nm to 83 nm with inimitable size (Figure **6**(**b**)) demonstrating the strong coordination of bonds between manganese and sulphur. At higher concentration of Mn-content, spherical shaped nano-particles were formed with distinct grain boundary and dimensions of these nanoparticles were observed to increase with crystal expansion along c axis [35]. For pure FeS thin films the growth of material was bit smooth and dispersed throughout the substrate surface however, the increase in doping concentration resulted in inclusion of voids due to agglomeration of materials at particular nucleation sites as shown in Figure **6**(**a**-**f**). The microstructural analysis is strongly corelated with the XRD data of manganese doped FeS samples. The SEM analysis revealed the grain size while XRD revealed the crystallite size. Grain is in fact collection of few crystallite hence larger in size as compared to the crystallites, the smallest unit of crystals.

3.3. Optical Properties

The optical characteristics of undoped and manganese doped FeS (mackinawite) thin films were studied using diffuse reflectance spectroscopy (DRS). It is obvious that when electrons of a material are excited by incident photons, it releases a photon of almost same energy when returned back to its original. The reflectance is purely a surface phenomenon and

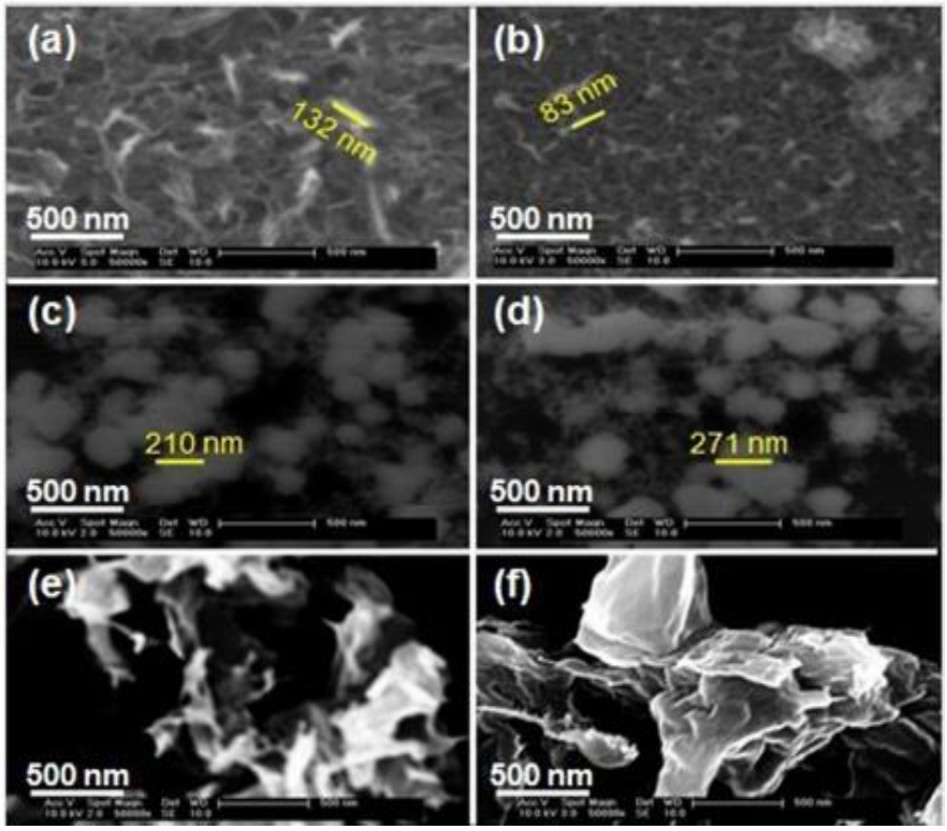

Figure 6: SEM micrographs of undoped and manganese doped FeS thin films (**a**) Undoped (**b**) **x=0.02** (**c**) **x=0.04** (**d**) **x=0.06** (**e**) **x=0.08** (**f**) **x=0.1**

depends upon opaqueness of thin films [39]. Inset of Figure **7** shows variations of reflectance spectra of undoped and manganese doped FeS (mackinawite) thin films within the wavelength range from 400 to 750 nm. It can be seen that pure FeS and $Fe_{0.98}Mn_{0.02}S$ thin films exhibit very low reflectance in visible region as compared to the thin films containing high concentration of manganese content [40]. Thin films with dopant concentrations as x=0.04 – 0.1 depicted high reflectance at 580 nm attributed to red shift. The increasing reflection demonstrated the higher number of free electrons that are weakly bound with their own atoms and opaqueness of the deposited thin films with higher doping concentrations of manganese [41].

Figure **7** shows the direct optical band gap of undoped and manganese doped mackinawite thin films by changing the reflectance values into absorption values using Kubelka-Munk (K-M) function as expressed below:

$$F(R_\infty) = \frac{(1-R_\infty)^2}{2R_\infty} \tag{7}$$

where R_∞ shows reflectance and F(R_∞) denote Kubelka-Munk (K-M) function [42]. Direct energy band gap was estimated using Tauc's plot as given below, plotting $hv\,(eV)$ on x-coordinate with $\left[F(R_\infty).hv\right]^2$ on y-coordinate and extrapolating the linear part of curve towards x-axis.

$$(ahv)^{\frac{1}{n}} = A(hv - Eg) \tag{8}$$

Here, α represents the absorption coefficient, h is planks constant, A is proportionality constant, incident light frequency is denoted by v, band gap energy is represented by Eg and n give the electronic transition nature which is $\frac{1}{2}$ to measure direct energy band gap.

It has been observed that small nano-crystalline size of intrinsic FeS thin films exhibt large optical band gap *i.e.* 2.23 eV which implies that there was less overlapping of energies level as results of small number of atoms or molecules that reduced the energy band width [28]. Figure **8** shows that energy band gap decreases from 2.23 to 1.89 eV as function of Mn-concentrations as listed in Table **1**, owing to associated

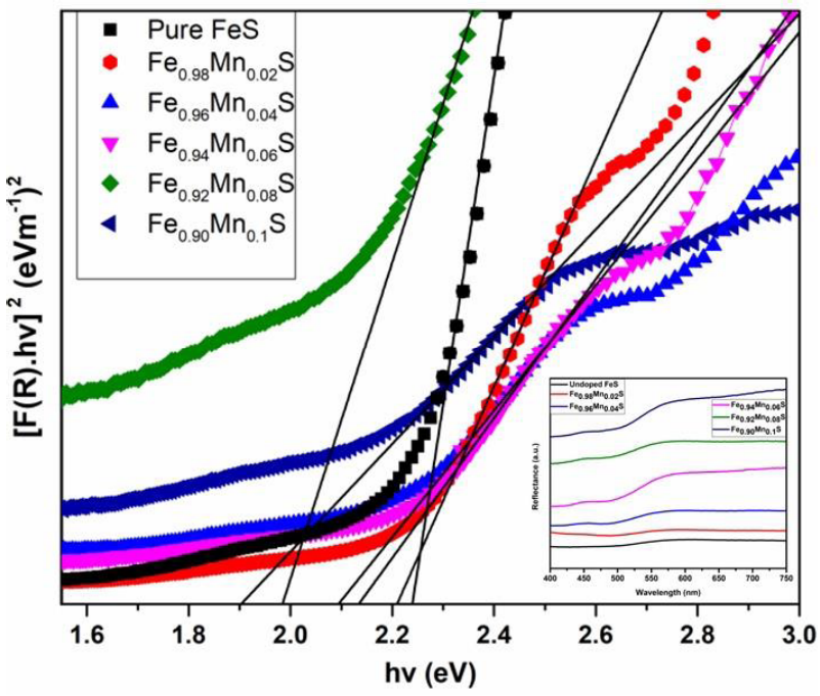

Figure 7: The $\left[F\left(R_{\infty}\right).hv\right]^2$ versus hv curves for pure and manganese doped thin films. Inset shows the reflectance spectra.

reasons such as crystallite size, electron–electron interaction and electron-impurities interactions [43]. The possible increase in number of charge carriers would also be a reason for narrowing of optical band gap in doped thin films. The electron–electron interactions provide small mean free path between conduction and localized electrons that give rises large overlapping of wavelengths when Mn-contents increased. Electron-impurities interaction also be the one of reasons for reduced optical band gap energy in Mn doped FeS thin films [44, 45].

4. CONCLUSIONS

Undoped and manganese doped FeS (mackinawite) thin films were synthesized using chemical Bath deposition (CBD) technique at 90°C for deposition time of three hours. XRD patterns revealed that thin films exhibit tetragonal structure of mackinawite like FeS that prevailed even after manganese doping claiming the phase and structure stability of deposited thin films. SEM micrographs confirmed the formation of nano-scale structures like nanoparticles, nanoflakes and nanoflowers with homogenous distribution. The FeS thin films with 2% of manganese doping exhibited large optical band gap energy with stable crystal structure. The inimitable morphology of deposited material would have potential to be used in optoelectronic devices specifically in solar cell applications.

REFERENCES

[1] Srivastava RP, Ingole S. An investigation on the phase purity of iron pyrite (FeS2) thin films obtained from the sulfurization of hematite (Fe2O3) thin films. Materials Science in Semiconductor Processing. 2020; 106: 104775. https://doi.org/10.1016/j.mssp.2019.104775

[2] Kılıç B, Roehling J, Özmen ÖT. Synthesis and Optoelectronic Properties of Pyrite (FeS2) Nanocrystals Thin Films for Photovoltaic Applications. Journal of Nanoelectronics and Optoelectronics. 2013; 8(3): 260-6. https://doi.org/10.1166/jno.2013.1462

[3] SM H. A Brief Review on the Polymer thin Film Solar Cells. 2016.

[4] Ritchie A, Bowles P, Scattergood D. Lithium-ion/iron sulphide rechargeable batteries. Journal of power sources. 2004; 136(2): 276-80. https://doi.org/10.1016/j.jpowsour.2004.03.043

[5] Al-Douri Y, Baaziz H, Charifi Z, Reshak AH. Density functional study of optical properties of beryllium chalcogenides compounds in nickel arsenide B8 structure. Physica B: Condensed Matter. 2012; 407(3): 286-96. https://doi.org/10.1016/j.physb.2011.09.127

[6] Al-Douri Y, Khachai H, Khenata R. Chalcogenides-based quantum dots: Optical investigation using first-principles calculations. Materials Science in Semiconductor Processing. 2015; 39: 276-82. https://doi.org/10.1016/j.mssp.2015.05.016

[7] Boudiaf K, Bouhemadou A, Boudrifa O, Haddadi K, Saoud FS, Khenata R, et al. Structural, Elastic, Electronic and Optical Properties of LaOAgS-Type Silver Fluoride Chalcogenides: First-Principles Study. Journal of Electronic Materials. 2017; 46(7): 4539-56. https://doi.org/10.1007/s11664-017-5452-6

[8] Rached D, Rabah M, Benkhettou N, Khenata R, Soudini B, Al-Douri Y, et al. First-principle study of structural, electronic and elastic properties of beryllium chalcogenides BeS, BeSe and BeTe. Computational materials science. 2006; 37(3):

292-9.
https://doi.org/10.1016/j.commatsci.2005.08.005

[9] Vaughan DJ, Lennie AR. The iron sulphide minerals: their chemistry and role in nature. Science Progress (1933-). 1991: 371-88.

[10] Vaughan DJ. Mineral chemistry of metal sulfides. Cambridge Earth Sci Ser, Cambridge. 1978; 493.

[11] Vaughan DJ. Nickelian mackinawite from Vlakfontein, Transvaal: A reply. American Mineralogist: Journal of Earth and Planetary Materials. 1970; 55(9-10): 1807-8.

[12] Tossell J, Vaughan D, Burdett J. Pyrite, marcasite, and arsenopyrite type minerals: Crystal chemical and structural principles. Physics and Chemistry of Minerals. 1981; 7(4): 177-84.
https://doi.org/10.1007/BF00307263

[13] Evans Jr HT, Milton C, Chao E, Adler I, Mead C, Ingram B, et al. Valleriite and the new iron sulfide, mackinawite. US Geological Survey Professional Paper. 1964; 475: 64-9.

[14] Csákberényi-Malasics D, Rodriguez-Blanco JD, Kis VK, Rečnik A, Benning LG, Pósfai M. Structural properties and transformations of precipitated FeS. Chemical Geology. 2012; 294: 249-58.
https://doi.org/10.1016/j.chemgeo.2011.12.009

[15] Berner RA. Iron sulfides formed from aqueous solution at low temperatures and atmospheric pressure. The Journal of Geology. 1964; 72(3): 293-306.
https://doi.org/10.1086/626987

[16] Berner RA. Tetragonal iron sulfide. Science. 1962; 137(3531): 669-.
https://doi.org/10.1126/science.137.3531.669.b

[17] Taylor P, Rummery T, Owen D. Reactions of iron monosulfide solids with aqueous hydrogen sulfide up to 160 C. Journal of Inorganic and Nuclear Chemistry. 1979; 41(12): 1683-7.
https://doi.org/10.1016/0022-1902(79)80106-2

[18] Rickard D, Griffith A, Oldroyd A, Butler IB, Lopez-Capel E, Manning D, et al. The composition of nanoparticulate mackinawite, tetragonal iron (II) monosulfide. Chemical Geology. 2006; 235(3-4): 286-98.
https://doi.org/10.1016/j.chemgeo.2006.07.004

[19] Lennie A, Redfern SA, Schofield P, Vaughan D. Synthesis and Rietveld crystal structure refinement of mackinawite, tetragonal FeS. De Gruyter; 1995.
https://doi.org/10.1180/minmag.1995.059.397.10

[20] Maji SK, Dutta AK, Biswas P, Karmakar B, Mondal A, Adhikary B. Nanocrystalline FeS thin film used as an anode in photo-electrochemical solar cell and as hydrogen peroxide sensor. Sensors and Actuators B: Chemical. 2012; 166: 726-32.
https://doi.org/10.1016/j.snb.2012.03.048

[21] Dickinson RG, Friauf JB. The crystal structure of tetragonal lead monoxide. Journal of the American Chemical Society. 1924; 46(11): 2457-63.
https://doi.org/10.1021/ja01676a015

[22] Mullet M, Boursiquot S, Abdelmoula M, Génin JM, Ehrhardt J-J. Surface chemistry and structural properties of mackinawite prepared by reaction of sulfide ions with metallic iron. Geochimica et cosmochimica acta. 2002; 66(5): 829-36.
https://doi.org/10.1016/S0016-7037(01)00805-5

[23] Jeong HY, Lee JH, Hayes KF. Characterization of synthetic nanocrystalline mackinawite: crystal structure, particle size, and specific surface area. Geochimica et cosmochimica acta. 2008; 72(2): 493-505.
https://doi.org/10.1016/j.gca.2007.11.008

[24] Denholme S, Demura S, Okazaki H, Hara H, Deguchi K, Fujioka M, et al. Evidence for non-metallic behaviour in tetragonal FeS (mackinawite). Materials Chemistry and Physics. 2014; 147(1-2): 50-6.
https://doi.org/10.1016/j.matchemphys.2014.04.005

[25] Wolthers M, Van der Gaast SJ, Rickard D. The structure of disordered mackinawite. American Mineralogist. 2003; 88(11-12): 2007-15.
https://doi.org/10.2138/am-2003-11-1245

[26] Rickard D, Luther GW. Chemistry of iron sulfides. Chemical reviews. 2007; 107(2): 514-62.
https://doi.org/10.1021/cr0503658

[27] Sines IT, Vaughn II DD, Misra R, Popczun EJ, Schaak RE. Synthesis of tetragonal mackinawite-type FeS nanosheets by solvothermal crystallization. Journal of Solid State Chemistry. 2012; 196: 17-20.
https://doi.org/10.1016/j.jssc.2012.07.056

[28] Malek TJ, Chaki SH, Deshpande M. Structural, morphological, optical, thermal and magnetic study of mackinawite FeS nanoparticles synthesized by wet chemical reduction technique. Physica B: Condensed Matter. 2018; 546: 59-66.
https://doi.org/10.1016/j.physb.2018.07.024

[29] Nozaki H, Nakazawa H, Sakaguchi K. Synthesis of mackinawite by vacuum deposition method. Mineralogical Journal. 1977; 8(7): 399-405.
https://doi.org/10.2465/minerj.8.399

[30] Shoesmith D, Bailey M, Ikeda B. Electrochemical formation of mackinawite in alkaline sulphide solutions. Electrochimica Acta. 1978; 23(12): 1329-39.
https://doi.org/10.1016/0013-4686(78)80013-9

[31] Hurma T, Aksay S. Investigations of Structural Vibrational and Optical Properties of Mackinawite Nanostructured FeS Film. Revista Română de Materiale/Romanian Journal of Materials. 2018; 48(1): 18-23.

[32] Akhtar MS, Alenad A, Malik MA. Synthesis of mackinawite FeS thin films from acidic chemical baths. Materials Science in Semiconductor Processing. 2015; 32: 1-5.
https://doi.org/10.1016/j.mssp.2014.12.073

[33] Kwon KD, Refson K, Sposito G. Transition metal incorporation into mackinawite (tetragonal FeS). American Mineralogist. 2015; 100(7): 1509-17.
https://doi.org/10.2138/am-2015-5211CCBYNCND

[34] Arakaki T, Morse JW. Coprecipitation and adsorption of Mn (II) with mackinawite (FeS) under conditions similar to those found in anoxic sediments. Geochimica et cosmochimica acta. 1993; 57(1): 9-14.
https://doi.org/10.1016/0016-7037(93)90463-7

[35] Zavašnik J, Stanković N, Arshad SM, Rečnik A. Sonochemical synthesis of mackinawite and the role of Cu addition on phase transformations in the Fe-S system. Journal of nanoparticle research. 2014; 16(2): 2223.
https://doi.org/10.1007/s11051-013-2223-z

[36] Wilkin RT, Beak DG. Uptake of nickel by synthetic mackinawite. Chemical Geology. 2017; 462: 15-29.
https://doi.org/10.1016/j.chemgeo.2017.04.023

[37] Prabukanthan P, Thamaraiselvi S, Harichandran G, Theerthagiri J. Single-step electrochemical deposition of Mn 2+ doped FeS 2 thin films on ITO conducting glass substrates: physical, electrochemical and electrocatalytic properties. Journal of Materials Science: Materials in Electronics. 2019; 30(4): 3268-76.
https://doi.org/10.1007/s10854-018-00599-w

[38] Echendu O, Werta S, Dejene F, Egbo K. Structural, vibrational, optical, morphological and compositional properties of CdS films prepared by a low-cost electrochemical technique. Journal of Alloys and Compounds. 2019; 778: 197-203.
https://doi.org/10.1016/j.jallcom.2018.11.130

[39] Osorio MF, Figueroa P, Prieto F, Boulanger P, Londoño E. A novel approach to documenting artifacts at the Gold Museum in Bogota. Computers & Graphics. 2011; 35(4): 894-903.
https://doi.org/10.1016/j.cag.2011.01.014

[40] Kirkeminde A, Ruzicka BA, Wang R, Puna S, Zhao H, Ren S. Synthesis and optoelectronic properties of two-dimensional FeS2 nanoplates. ACS applied materials & interfaces. 2012; 4(3): 1174-7. https://doi.org/10.1021/am300089f

[41] Yu Q, Cai S, Jin Z, Yan Z. Evolutions of composition, microstructure and optical properties of Mn-doped pyrite (FeS2) films prepared by chemical bath deposition. Materials Research Bulletin. 2013; 48(9): 3601-6. https://doi.org/10.1016/j.materresbull.2013.05.074

[42] Kortüm G, Braun W, Herzog G. Principles and techniques of diffuse-reflectance spectroscopy. Angewandte Chemie International Edition in English. 1963; 2(7): 333-41. https://doi.org/10.1002/anie.196303331

[43] Gibbs ZM, LaLonde A, Snyder GJ. Optical band gap and the Burstein-Moss effect in iodine doped PbTe using diffuse reflectance infrared Fourier transform spectroscopy. New Journal of Physics. 2013; 15(7): 075020. https://doi.org/10.1088/1367-2630/15/7/075020

[44] Saw K, Aznan N, Yam F, Ng S, Pung S. New insights on the burstein-moss shift and band gap narrowing in indium-doped zinc oxide thin films. PloS one. 2015; 10(10): e0141180. https://doi.org/10.1371/journal.pone.0141180

[45] Bhattacharjee A, à la Guillaume CB. Model for the Mn acceptor in GaAs. Solid state communications. 1999; 113(1): 17-21. https://doi.org/10.1016/S0038-1098(99)00438-X

Received on 16-06-2022 Accepted on 02-08-2022 Published on 06-09-2022

DOI: https://doi.org/10.31875/2410-4701.2022.09.03

© 2022 Yaqoob *et al.*; Zeal Press.
This is an open access article licensed under the terms of the Creative Commons Attribution License (http://creativecommons.org/licenses/by/4.0/) which permits unrestricted use, distribution and reproduction in any medium, provided the work is properly cited.